Neuron

NeuroResource

Dynamic Functional Connectivity of Resting-State Spinal Cord fMRI Reveals Fine-Grained Intrinsic Architecture

Graphical Abstract

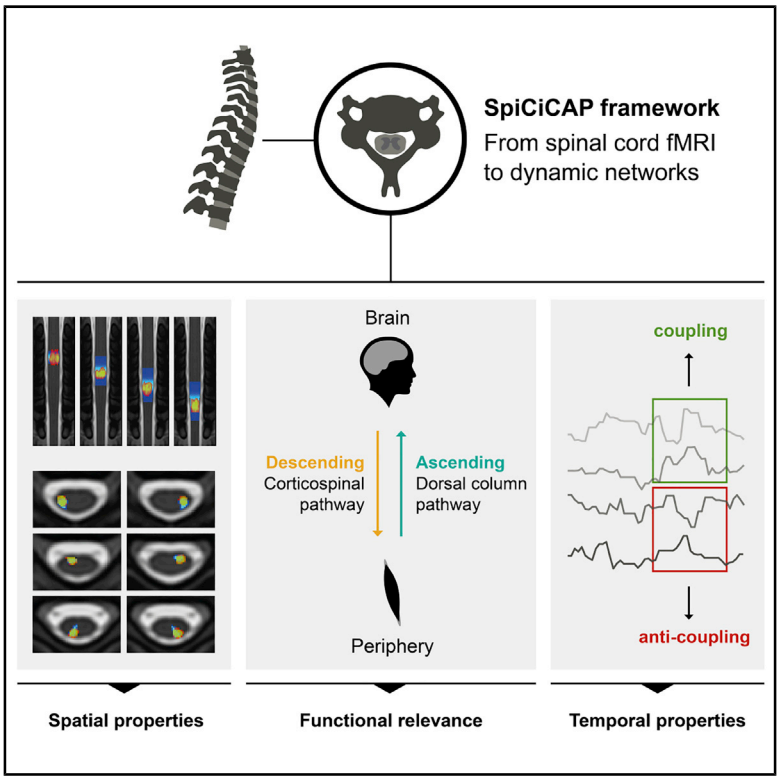

Highlights

- The SpiCiCAP framework can delineate functional spinal circuits in fMRI data
- Components are revealed that are highly structured and in line with neuroanatomy
- Network organization emerges based on ascending and descending spinal neural pathways
- Pathway-specific patterns of temporal properties are highlighted

Authors

Nawal Kinany, Elvira Pirondini, Silvestro Micera, Dimitri Van De Ville

Correspondence

silvestro.micera@epfl.ch (S.M.), dimitri.vandeville@epfl.ch (D.V.D.V.)

In Brief

Kinany et al. introduce the SpiCiCAP framework, a dynamic functional connectivity approach to disentangle spinal functional activity acquired using fMRI. They demonstrate the potential of this methodology to uncover fine-grained features of the spinal cord's functional architecture and to explore their physiological relevance.

Kinany et al., 2020, Neuron *108*, 424–435
November 11, 2020
https://doi.org/10.1016/j.neuron.2020.07.024

CellPress

CellPress

Neuron

NeuroResource

Dynamic Functional Connectivity of Resting-State Spinal Cord fMRI Reveals Fine-Grained Intrinsic Architecture

Nawal Kinany,[1,2] Elvira Pirondini,[3] Silvestro Micera,[2,4,5,*] and Dimitri Van De Ville[1,3,5,6,*]

[1]Medical Image Processing Laboratory, Center for Neuroprosthetics, Institute of Bioengineering, Ecole Polytechnique Fédérale de Lausanne (EPFL), 1202 Geneva, Switzerland

[2]Bertarelli Foundation Chair in Translational Neuroengineering, Center for Neuroprosthetics, Institute of Bioengineering, Ecole Polytechnique Fédérale de Lausanne (EPFL), 1202 Geneva, Switzerland

[3]Department of Radiology and Medical Informatics, University of Geneva, 1211 Geneva, Switzerland

[4]The BioRobotics Institute and Department of Excellence in Robotics and AI, Scuola Superiore Sant'Anna, 56025 Pontedera, Italy

[5]These authors contributed equally

[6]Lead Contact

*Correspondence: silvestro.micera@epfl.ch (S.M.), dimitri.vandeville@epfl.ch (D.V.D.V.)

https://doi.org/10.1016/j.neuron.2020.07.024

SUMMARY

The neuroimaging community has shown tremendous interest in exploring the brain's spontaneous activity using functional magnetic resonance imaging (fMRI). On the contrary, the spinal cord has been largely overlooked despite its pivotal role in processing sensorimotor signals. Only a handful of studies have probed the organization of spinal resting-state fluctuations, always using static measures of connectivity. Many innovative approaches have emerged for analyzing dynamics of brain fMRI, but they have not yet been applied to the spinal cord, although they could help disentangle its functional architecture. Here, we leverage a dynamic connectivity method based on the clustering of hemodynamic-informed transients to unravel the rich dynamic organization of spinal resting-state signals. We test this approach in 19 healthy subjects, uncovering fine-grained spinal components and highlighting their neuroanatomical and physiological nature. We provide a versatile tool, the spinal innovation-driven co-activation patterns (SpiCiCAP) framework, to characterize spinal circuits during rest and task, as well as their disruption in neurological disorders.

INTRODUCTION

Since its early days in the 1990s, functional magnetic resonance imaging (fMRI) has had a tremendous impact on the field of neuroscience, substantially advancing our understanding of the central nervous system (CNS). Relying on non-invasive detection of blood-oxygen-level-dependent (BOLD) signal changes, this imaging technique offers meaningful insights into the underlying neuronal activity (Logothetis et al., 2001). As such, it has been widely deployed to investigate system-level brain function, not only during tasks but also at rest, with fMRI studies focusing on the spontaneous fluctuations of the BOLD signals (van den Heuvel and Hulshoff Pol, 2010). In this context, resting-state networks (RSNs) are conventionally extracted using functional connectivity (FC) measures based on the coherent activation (e.g., Pearson correlation) of distinct brain regions. These intrinsic networks have emerged as the building blocks of human brain function (Damoiseaux et al., 2006), and their activity has been shown to encode a wide array of behavioral traits, from emotion to intellectual performances (Greicius et al., 2003; Liégeois et al., 2019). Besides, their widespread alteration in neurological diseases also support their clinical relevance and their potential as biomarkers of functional integrity (Allali et al., 2018; Castellanos et al., 2013). Unfortunately, this exploration of the functional architecture of the human CNS *in vivo* has been essentially focused on the brain. In contrast, the spinal cord, another component of the CNS, has been mostly overlooked, even though this structure plays a crucial role in sensorimotor processing, for instance in proprioception, pain processing, or during movement generation and control (Darby and Frysztak, 2013). As such, insights into the intrinsic functional organization of human spinal circuits appear as pivotal contributions to fundamental and clinical neurosciences.

This limited amount of research may partly stem from the inaccessibility of the spinal cord, a small structure deeply encapsulated in the vertebral column (Marieb and Hoehn, 2014; Powers et al., 2018). Imaging this region is indeed particularly challenging, as the adjacent bones and organs make it prone to field inhomogeneities and physiological noise (Giove et al., 2004; Stroman et al., 2014). This may explain why functional activity

of the spinal cord was, at first, mainly explored using indirect peripheral measurements (e.g., muscle activity, force, reflexes, or sensory tests) (Greenberg, 2003; Knikou, 2008; Yakovenko et al., 2002). Yet, developments in spinal cord fMRI acquisition (Finsterbusch, 2013) and processing protocols (Eippert et al., 2017a; De Leener et al., 2017) have worked toward circumventing these constraints, and a growing body of research highlighted the feasibility of this approach (Wheeler-Kingshott et al., 2014). Moreover, the validity of BOLD signals as a hemodynamic proxy of spinal neural activity was recently confirmed in non-human primates, as signal variations were shown to be in agreement with electrophysiological activity (i.e., local field potentials) (Wu et al., 2019).

Spinal cord fMRI studies have primarily focused on task-evoked activity, offering an unparalleled opportunity to examine the human spinal cord in action (Wheeler-Kingshott et al., 2014). Spontaneous signal fluctuations, on the other hand, were only explored in recent years. Sensory and motor RSNs were first reported using different approaches, such as seed-based FC (at 3T, Eippert et al., 2017b; and at 7T, Barry et al., 2014, 2016) or independent component analysis (ICA) (at 3T; Kong et al., 2014). Similar components were also identified at ultra-high field (9.4T) in rats (Wu et al., 2018) and non-human primates (Chen et al., 2015). Although these studies demonstrated the existence of functional circuits in the spinal cord at rest, their neurophysiological underpinnings remained unclear (Eippert and Tracey, 2014).

A critical factor that hindered thorough characterization of the nature of spinal networks was the use of static measures of FC, as all earlier studies assumed temporal stationarity over the scanning session. As a result, they did not consider the dynamic evolution of interactions over time, and they could not fully capture the properties of functional networks (Calhoun et al., 2001). In the brain, however, it has been highlighted that FC fluctuates at the timescale of seconds, and numerous dynamic FC (dFC) approaches have been proposed to delve into these time-varying properties (Preti et al., 2016). This finding has provided new insights into the properties of resting-state (RS) signals, as well as informed on the disrupted dynamic interplay of distinct brain regions in various neurological disorders.

Here, we posit that dynamic methods could enable disentangling the ongoing sustained spinal activity, possibly revealing new attributes of spinal RSNs. To this end, we leveraged a promising approach to extract dynamic RS components, termed innovation-driven co-activation patterns (iCAPs). In this context, the term innovation refers to transient activity, which is recovered using robust hemodynamic-informed deconvolution (Karahanoğlu et al., 2013). Patterns obtained using transients constitute the building blocks of time-resolved activity and offer a unique way to temporally dissect overlapping signals. Notably, this has previously enabled the separation of known brain RSNs (e.g., the default mode network) into multiple subsystems (Karahanoğlu and Van De Ville, 2015). Capitalizing on this potential to unfold ongoing functional activity, we combined this method with a dedicated spinal cord fMRI pipeline into the spinal iCAP (SpiCiCAP) framework. Using this framework, we assessed spatial and temporal properties of cervical RS activity in healthy participants and uncovered precise features of the spinal cord functional architecture. To the best of our knowledge, this is the first time that fine-grained RS components are revealed in the spinal cord. This unparalleled level of detail allowed us to shed new light on their neuroanatomical nature, as well as to further characterize their physiological roles and, hence, emphasize their involvement in distributed neural pathways supporting ascending sensory feedback (e.g., for proprioception) and descending communication from supraspinal structures (e.g., for motor control). The SpiCiCAP framework could foster relevant advances in our understanding of spinal cord function, not only at rest but also when dynamically modulated in sensory and motor tasks. Finally, this framework opens an avenue to map spinal circuits in neurological conditions and to investigate the mechanisms associated with dysfunction and recovery.

RESULTS

The SpiCiCAP Framework

Our goal was to achieve a deeper understanding of spinal cord's functional architecture. To this end, we reasoned that exploring the time-varying content of spinal spontaneous fluctuations would bring new light on their neurophysiological nature. The SpiCiCAP framework, whose approach is outlined in Figure 1, integrates tailored spinal cord fMRI protocols with a state-of-the-art method to extract dynamic RSNs by using clustering of hemodynamic-informed transients. It enables us the ability to decompose spinal circuits and to investigate their spatiotemporal properties.

Spatial Maps of Spinal iCAPs Specifically Match Spinal Cord Neuroanatomy

Using the SpiCiCAP framework, we extracted spinal iCAPs for two levels of granularity (i.e., temporal clustering done independently for two different parameters K, 4 or 40, corresponding to the number of iCAPs; see Figure 1). The choice of these two levels of granularity was supported by a systematic evaluation of clustering reproducibility for different Ks (details presented in Figure S3). Visual inspection of the recovered iCAPs confirmed the absence of noisy spatial patterns (Figure 2). Components displayed high spatial segregation, as underlined by the limited overlap between iCAP maps (Figure S5). In line with previous studies (Kong et al., 2014; Weber et al., 2018), spinal iCAPs spanned a limited rostro-caudal extent, likely reflecting the segmental structure of the spinal cord. Specifically, low-level granularity iCAPs corresponded to spinal levels C5 to C8 (Figure 2B), with on average 91% of their voxels in a single spinal level (Figure S5). The specificity of the matching between iCAPs and segmental borders was confirmed using Dice coefficients (mean ± SD = 0.71 ± 0.03). For this low-level granularity, all iCAPs were bilateral and included dorsal and ventral components (Figure S4). When increasing the granularity to 40 iCAPs, we observed that components were further subdivided within the axial plane (Figure 2C), with high-granularity iCAPs that were predominantly unilateral and strictly confined to either the dorsal or ventral side. To achieve a comprehensive description of this axial organization, we harnessed a detailed atlas of the spinal cord (Lévy et al., 2015; Figure S2) to precisely quantify the axial voxel distribution. For each of these fine-grained iCAPs, voxels

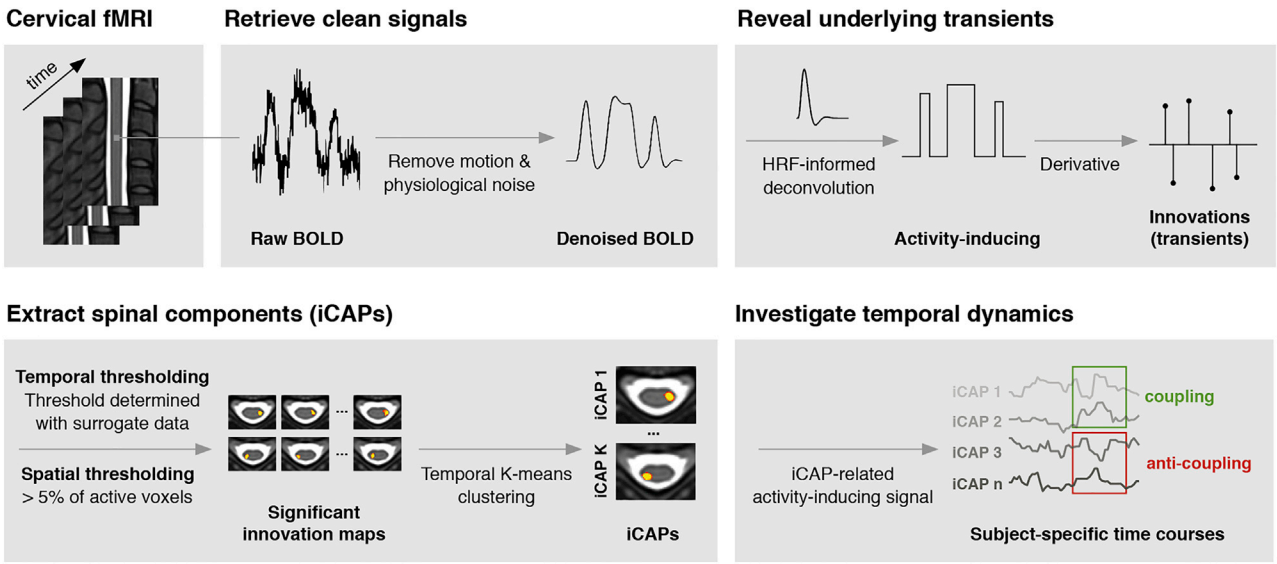

Figure 1. SpiCiCAP Framework

Cervical functional images are processed to circumvent the effect of various sources of noise. Hemodynamic blur is removed using hemodynamic-informed deconvolution to reveal activity-inducing signals. Innovation signals (i.e., transients) are then obtained by temporal derivation. A two-step thresholding is applied to select significant innovation frames, which undergo K-means temporal clustering to obtain stable iCAPs (K, number of iCAPs). Recovered iCAPs can be used as regions of interest to extract subject-specific time courses from activity-inducing signals. Finally, interaction measures (e.g., Jaccard index for couplings and anti-couplings) can be computed. Inspired by Karahanoğlu et al. (2013).

were distributed over a restricted number of atlas regions (on average, two regions per iCAP included 68% of its voxels; Figure S5), emphasizing that the activity patterns were highly localized and structured. Each spinal component was, thus, matched to a specific atlas region (mean Dice coefficient ± SD = 0.61 ± 0.11). Overall, these results illustrated the high correspondence between the components extracted using the SpiCiCAP framework and the underlying neuroanatomy of the spinal cord.

Spinal iCAPs Assemble into Neural Pathways

To further inspect the neuroanatomical identity of the 40 spinal iCAPs, we used the hard assignment proposed above (i.e., each iCAP uniquely matched with an atlas region) and computed the number of iCAPs found in each of the atlas regions, so as to seek whether an organized topographical distribution could be highlighted (Figure 3). We observed that iCAPs fell into a limited number of regions, i.e., 12 of the 36 atlas regions (see Figure S2 for the exhaustive list), which corresponded to six distinct neuroanatomical zones comprising both gray (i.e., ventral horns and intermediate regions) and white matter (i.e., the dorsal column, formed by the fasciculus gracilis, and fasciculus cuneatus, the cortico-spinal tract, and the medial lemniscus). For each of them, iCAPs were present in both left and right lateralization. We then investigated whether this apparent sparsity, driven by fMRI activity, had a functional meaning. An examination of the different roles of these regions (Figure S2; Darby and Frysztak, 2013) revealed that iCAPs were essentially organized following two neural pathways of the spinal cord: 18 iCAPs relied on the cortico-spinal tract pathway (CST), whereas 16 iCAPs corresponded to the dorsal column-medial lemniscus pathway (DCML) (Figure 3A). These pathways fulfill distinct functional contributions (Figure 3B), as they are involved in conveying and processing signals from (e.g., for motor control) and to (e.g., for proprioception) the brain, respectively (Darby and Frysztak, 2013). The former is a descending pathway that goes from the motor cortex to the ventral horns (regions 31–32), through the cortico-spinal tract (regions 5–6). The latter is an ascending pathway, sending proprioceptive and sensory information from the periphery to the somatosensory cortex by traveling through the dorsal column (regions 1–4) and the medial lemniscus (regions 13–14). Finally, 6 iCAPs were found in the intermediate zone, INTER (regions 33–34), at the interface between these ascending and descending pathways. The rostro-caudal distribution of the iCAPs underlined a uniform presence of ascending and descending pathways from C5 to C8, whereas no intermediate regions were found in C8 (Figure 3C). To evaluate the distance between iCAPs along the two pathways, we computed the mean rostro-caudal position of the associated iCAPs in each spinal level. The average spatial gaps along the CST and DCML were 17.88 ± 1.70 mm and 18.43 ± 0.6 mm (mean ± SD over spinal levels), respectively, which are in line with the anatomical distance between spinal levels (Cadotte et al., 2015). In summary, these results suggested that the recovered spinal iCAPs were functionally relevant. This idea hints at the potential of the proposed framework to non-invasively monitor the neural mechanisms underlying information flow and processing, both locally in the spinal cord and in relation to inputs from the brain and the periphery.

Spinal Functional Organization Is Stable within and between Subjects

We evaluated the consistency of the observed iCAPs both within and between subjects. First, we assessed the intra-subject

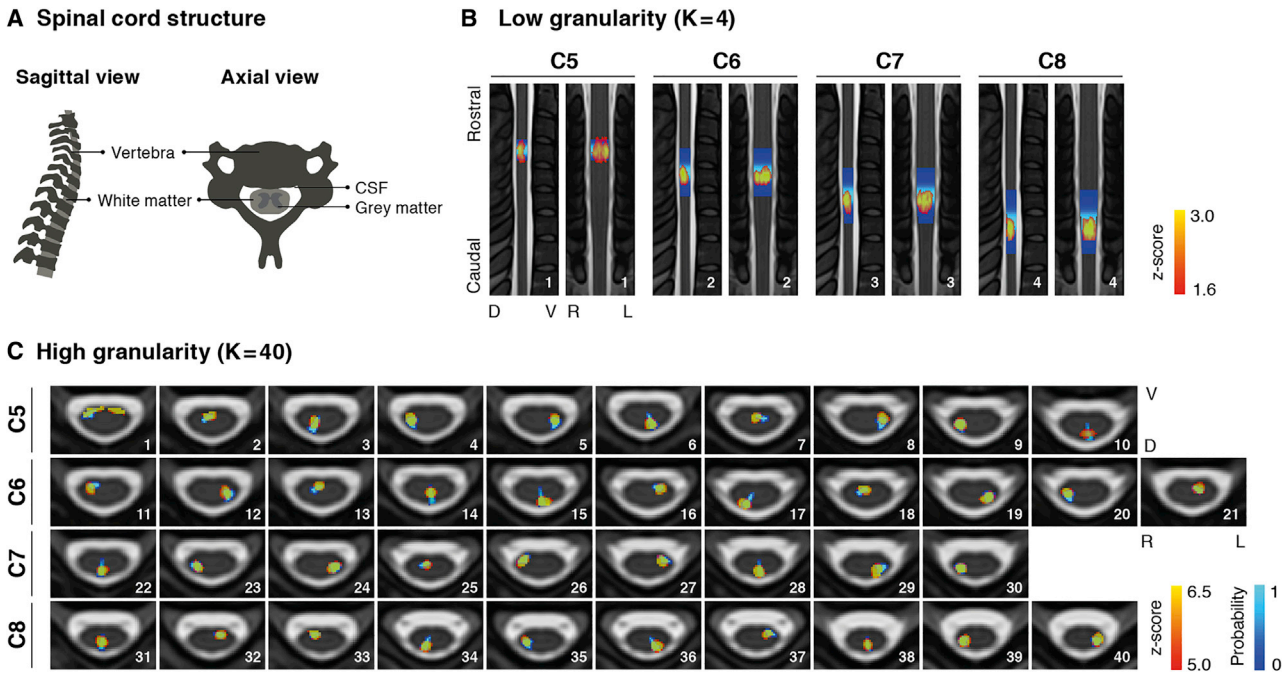

Figure 2. iCAPs Spatial Patterns

(A) Schematic representation of the structure of the spinal cord. CSF, cerebrospinal fluid.

(B) Each low-granularity iCAP spans a limited rostro-caudal extent, in line with the segmental structure of the spinal cord (one iCAP corresponds to one spinal level, mean Dice coefficient ± SD = 0.71 ± 0.03). Axial views are presented in Figure S4.

(C) When extracting 40 spinal iCAPs (presented from rostral to caudal components), spatial maps get divided within the axial plane and lined up with known subdivisions of the spinal cord, reflecting meaningful neuroanatomical structures (Figure S2), such as white matter tracts or gray matter horns (mean Dice coefficient ± SD = 0.61 ± 0.11). Coronal and sagittal views are presented in Figure S4. Thresholded iCAP maps, in red, are overlaid on the corresponding spinal level or atlas region probabilistic maps, in blue (De Leener et al., 2017). The PAM50 template is used as a background (De Leener et al., 2018). ICAPs numbers are indicated in the bottom right corners. L, left; R, right; D, dorsal; V, ventral.

stability by splitting each subject's dataset into two equal parts (180 volumes each, i.e., 7.5 min) in which we recomputed iCAPs independently (Figure 4A). The intra-subject stability was particularly high for the low-granularity iCAPs (mean Dice coefficient ± SD of 0.83 ± 0.08), indicating that the coarse functional organization was stable over time within the same subjects. Conversely, the stability of fine-grained spatial patterns was more variable (mean Dice coefficient ± SD of 0.38 ± 0.20), with 12 iCAPs displaying Dice coefficients superior to 0.5 (maximum value of 0.84), whereas 7 iCAPs exhibited coefficients lower than 0.2 (minimum value of 0.06). ICAPs with low and high Dice coefficients were distributed over the different pathways, with no specific pattern. Despite this variability, both sets of iCAPs were in line with the underlying neuroanatomy (mean Dice coefficient with atlas regions ± SD of 0.63 ± 0.10 for part 1 and 0.61 ± 0.10 for part 2). Moreover, they carried similar functional relevance, as atlas regions of the two parts could still be clustered into the same pathways (ascending DCML, descending CST, and intermediate INTER) (Figure S6). We then probed inter-subject stability by comparing the iCAPs maps of all subjects for each iCAP pair of the full dataset. The spatial patterns were similar across subjects (Figure 4B), as highlighted by the diagonal matrices obtained for low- and high-granularity iCAPs (mean Dice coefficient ± SD of 0.49 ± 0.05 and 0.51 ± 0.06 for the different levels of granularity, respectively). Altogether, these findings underlined the stability of the spinal cord's functional organization, along with the potential of iCAPs to represent its underlying building blocks.

Dynamic Temporal Interactions Are Observed between iCAPs

Capitalizing on this stable spatial organization, we probed the temporal features of the 40 fine-grained spinal iCAPs. Each iCAP occurrence lasted on average 2.71 ± 0.15 volumes (mean over iCAPs ± SD, no significant difference between iCAPs), for a total duration of activation (positive and negative occurrences) of 27.42% ± 1.82% (mean over iCAPs ± SD, percentage of run length, no significant difference between iCAPs). A substantial amount of temporal overlap was observed between iCAPs, with an average of 10.97 ± 0.17 co-active iCAPs at each time point (mean over subjects ± SE; Figure 5A). To better understand the features of this large temporal overlap, we explored the (anti-) couplings between the 40 iCAPs (Figures 5B–5D). Overall, couplings (mean Jaccard index over subjects ± SE = 0.15 ± 0.007) were significantly stronger than anti-couplings (0.04 ± 0.003, $p < 0.001$), and they exhibited distinct behaviors. Specifically, larger couplings were observed within level (0.17 ± 0.005) than between levels (0.13 ± 0.004, $p < 0.001$). Conversely, anti-couplings were more prominent between levels (0.05 ± 0.002) than within level (0.03 ± 0.002, $p < 0.001$). This notable interplay

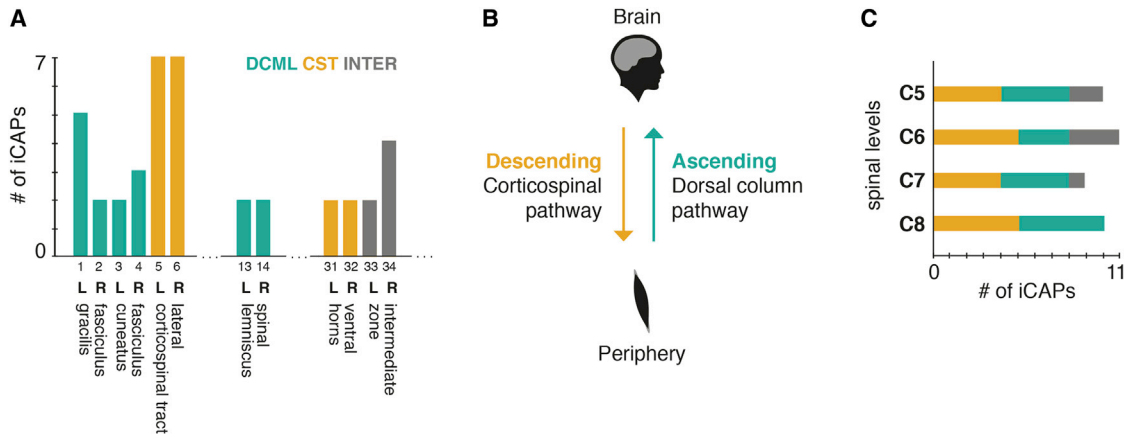

Figure 3. Neural Pathways

(A) Each fine-grained iCAPs was matched to one of the 36 atlas regions (hard assignment based on the maximum number of voxels, see Figures S2 and S5 for the details of the atlas regions and voxel distributions). The number of iCAPs per atlas region is presented, omitting regions with no assigned iCAP. Atlas regions from 1 to 30 correspond to the white matter, and regions from 31 to 36 are found in the gray matter. ICAPs cluster into spinal neural pathways involved in transmitting and processing information from and to the brain (DCML, dorsal column medial lemniscus pathway; CST, cortico-spinal tract pathway). Intermediate regions (INTER) are also present.

(B) Schematic representation of the spinal neural pathways.

(C) ICAP distribution in the different spinal levels. Colors refer to neural pathways.

between spinal iCAPs was stable across subjects, both for couplings (mean cosine similarity over subjects ± SE of 0.88 ± 0.01) and anti-couplings (0.76 ± 0.01). These results corroborated the hypothesis that spinal cord spontaneous fluctuations are highly entwined, prompting the need for dynamic approaches to dissect this activity.

iCAPs of Different Neural Pathways Exhibit Distinct Interplays

Finally, we examined the interactions between iCAPs grouped according to their neural relevance (ascending, descending, or intermediate), to potentially uncover distinctions regarding their coupling properties. Interaction profiles specific to each pathway (i.e., between the iCAPs belonging to the same pathway; Figure 6A) were highlighted, in particular in terms of within-level interactions. Couplings appeared larger inside the intermediate zone, whereas they were smaller in the ascending and descending pathways, especially for the former. Anti-couplings followed an opposite trend. The strong coupling inside the intermediate zone might be attributed to commissural interneurons, whose axons cross the midline to link the two hemicords. When assessing the interactions shared across pathways (i.e., between the iCAPs belonging to different pathways; Figure 6B), we found that the intermediate zone was differently coupled with the two others pathways, with stronger couplings occurring with the ascending regions. Anti-couplings, however, did not display any clear tendency. To further investigate whether these distinctions were inherent properties of connectivity inside and across neural pathways, we attempted to classify them using the aforementioned features (couplings and anti-couplings, within and between levels). We were able to distinguish interactions occurring inside the ascending and intermediate pathways, as they could be discriminated with high accuracy (73.7%, $p < 0.01$ and 63.2%, $p < 0.05$, respectively; non-parametric permutation testing against chance level, i.e., ~33.3%), confirming their distinct behaviors. Internal couplings within the descending pathways exhibited a more hybrid profile, resulting in a lower classification accuracy (52.6%, not significant). When looking at the interactions across neural pathways, we found the highest accuracy for the relationship between the ascending and descending pathways (63.3%, $p < 0.01$), although the interactions across the intermediate zones and the two other pathways could also be classified (57.9%, $p < 0.05$). This finding suggests that peculiar interactions exist between pathways, as they are engaged to support disparate sensorimotor functions.

DISCUSSION

In previous work, RSNs were shown to be a feature of the entire CNS, with the spinal cord demonstrating an intrinsic functional organization akin to the recognized brain's functional architecture (van den Heuvel and Hulshoff Pol, 2010). Although this organization has been presumed to support sensory, motor, or autonomic functions, its neurophysiological purpose has so far remained elusive. Former studies had solely focused on static FC, which merely reflects the average organization over the course of a functional run. In this regard, exploiting the dynamic features of spinal spontaneous activity could promote new insights into its physiological nature. In this study, we leveraged state-of-the-art spinal cord fMRI protocols, combined with a dFC method (Karahanoğlu and Van De Ville, 2015), and deployed the SpiCiCAP framework to unweave spinal RS fluctuations. We showed that these fluctuations were highly structured and could be precisely delineated into neuroanatomically relevant components. To the best of our knowledge, this is the first time that such fine-grained subdivisions of the spinal cord have been extracted using fMRI measures and, in particular,

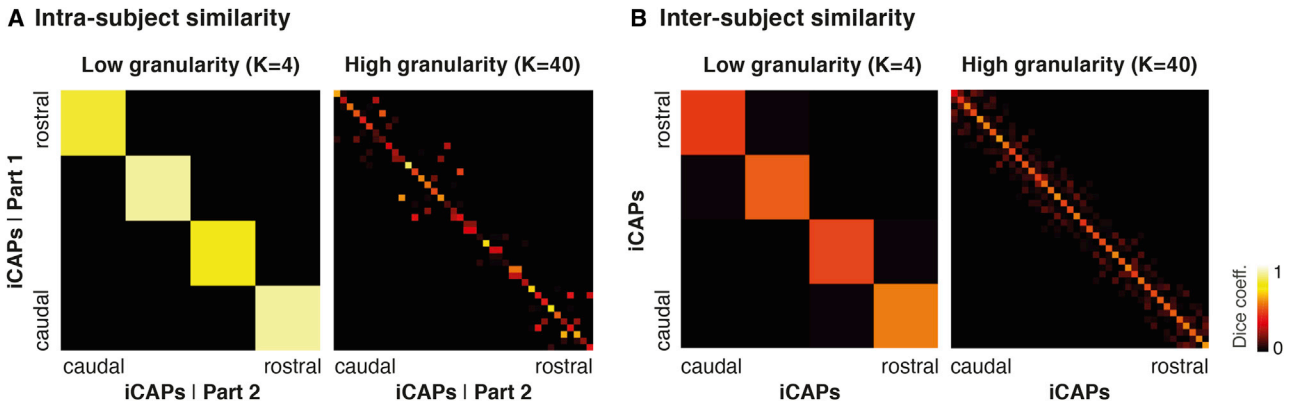

Figure 4. Stability of Spatial Patterns

(A) To evaluate the intra-subject stability of the iCAPs spatial maps, the dataset was split into two equal parts (180 volumes each, i.e., 7.5 min), and iCAPs were then computed independently for each part. The matrices show the Dice coefficients between both sets of iCAPs, for the two granularity levels (K = 4, low granularity; and K = 40, high granularity).

(B) The inter-subject stability was computed as the mean Dice coefficients over each pair of subjects, for a particular iCAP pair. In all matrices, iCAPs are ordered rostro-caudally.

RS activity. Thanks to this unprecedented level of detail, our results shed new light on the functional relevance of spinal fluctuations, underscoring their association with the main spinal neural pathways. Hereafter, we discuss these findings with an emphasis on their clinical potential.

Methodological Aspects

In this work, we deployed a dFC approach to exploit the richness of spontaneous spinal activity. Specifically, the SpiCiCAP framework first uses a tailored processing pipeline on spinal cord fMRI data. Regularized deconvolution of denoised time courses is then applied to retrieve the underlying activity-inducing signals, which is subsequently used to reveal robust transient activity (see Figure 1 for a summary of the different steps) (Karahanoğlu et al., 2013; Karahanoğlu and Van De Ville, 2015). Transients encode changes in the BOLD time courses (i.e., activations and de-activations) and can be used to determine components reflecting consistent patterns of co-activation, the so-called iCAPs. A unique feature of this method is its ability to disentangle spatially and temporally overlapping signals. In this study, fine-grained components could be revealed, suggesting that spinal activity manifests complex and non-stationary temporal properties that are better unraveled using a dynamic approach instead of conventional static methods. To thoroughly characterize iCAPs, we relied on maps of spinal levels and atlas regions (Cadotte et al., 2015; De Leener et al., 2017; Lévy et al., 2015), which enabled a systematic assessment of each component's physiological relevance (Figure S2). Notably, inter-subject variability is not represented in the atlas, but differences were assumed not to be critical at this spatial resolution. Although the SpiCiCAP framework offers unique advantages, certain drawbacks should be highlighted. First, this clustering-based approach implies that the number of clusters K should be *a priori* defined. Here, we selected K based on anatomical knowledge and reproducibility analyses, although this selection is not exclusive. Another aspect that should be considered pertains to the estimation of the hemodynamic response function (HRF). Indeed, the deconvolution step, which is deployed to recover activity-inducing signals (Figure 1), uses a single canonical HRF. Yet, the HRF is known to vary across subjects and regions (Hanwerker et al., 2004). Although these differences have not been closely investigated in the spinal cord, one study highlighted that the spinal HRF may be slower than in the brain (Giulietti et al., 2008). Besides, variations of the hemodynamic response between gray and white matter could also be probed, as differences in this regard have been demonstrated in the brain (Li et al., 2019). This topic warrants further investigation, and potential improvements to the SpiCiCAP framework could include a variable HRF model or integrate HRF identification within the deconvolution step. Finally, future research could examine the impact of changes in the processing pipeline (e.g., physiological noise removal, smoothing, etc.) on the reproducibility of spinal iCAPs, similar to how Eippert et al. (2017b) investigated robustness of static connectivity.

To foster the emergence of new research characterizing spinal functional pathways, we are providing our dataset and analysis pipeline as resources for the neuroscientific community. Spinal cord fMRI is still an emerging field, and currently, no such open dataset is publicly available. Despite significant improvements in the last years, spinal cord fMRI remains challenging and some limitations should be acknowledged, notably in terms of image quality. For instance, field inhomogeneities can lead to distortion and signal dropouts, although the extent of these signal variations was limited (Figure S1). It should also be noted that the low temporal resolution (repetition time [TR] = 2.5 s) might impede the detection of fast transients.

Spinal RS Components Are Highly Structured and Robust

The SpiCiCAP framework was used to explore spinal RS fluctuations by using two separate levels of granularity (i.e., either 4 low-granularity or 40 high-granularity iCAPs were extracted). All iCAPs presented spatially segregated patterns (Figure S5) and a limited rostro-caudal extent (Figures 2 and S4), corroborating previous results reporting that ICA-derived components

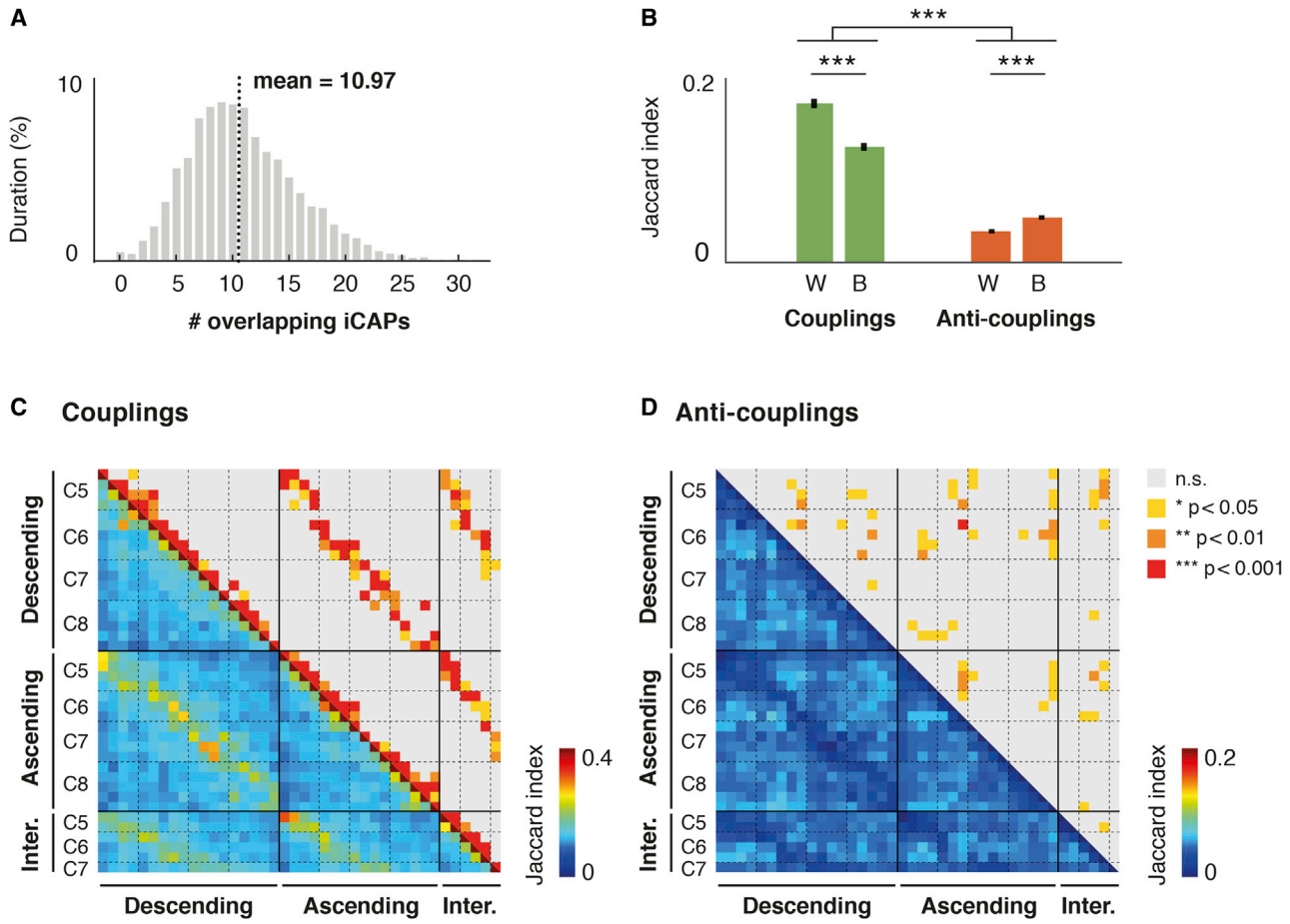

Figure 5. Investigating Temporal Overlap between iCAPs

(A) Percent duration of different degrees of co-activation (i.e., number of overlapping iCAPs), with respect to the total run duration. The dotted line indicates the mean over subjects.

(B) After extraction of the subject-specific time courses, interactions between iCAPs were assessed using Jaccard index (both for couplings, see C; and for anti-couplings, see D) Strong couplings were found between the different regions, mainly at the same spinal levels. Anti-couplings are weaker and mostly observed between spinal levels. Means over subjects ± SE are presented. W, within; B, between. ***p < 0.001, paired t test, Bonferroni corrected.

(C and D) For each matrix, iCAPs are grouped into ascending, descending, and intermediate regions and are ordered rostro-caudally for each category (dashed lines indicate the different spinal levels). The mean over subjects is presented. Bottom triangular matrices show Jaccard index for each pair of iCAPs, and top triangular matrices highlight significant interactions (non-parametric permutation testing, corrected for multiple comparisons).

did not span more than one vertebra (Kong et al., 2014). Here, we could further confirm that each low-granularity iCAP coincided with a single spinal level, from C5 to C8 (Figure 2B). A most striking observation was that increasing the granularity to 40 iCAPs allowed us to uncover fine-grained spinal components extending beyond the commonly reported dorso-ventral division (Figure 2C). These components were in close agreement with the underlying neuroanatomy and could be matched with a specific gray or white matter region. In line with previous studies, we observed components corresponding to the ventral (i.e., motor) horns (Barry et al., 2014; Kong et al., 2014; Liu et al., 2016; Weber et al., 2018). No iCAPs were, instead, assigned to the dorsal (i.e., sensory) horns, although few voxels were indeed present in these regions (Figure S5, regions 35 and 36). FC in the dorsal horns was previously reported as weaker and harder to reliably detect (Barry et al., 2016, 2018; Eippert et al., 2017b), possibly because of their narrow geometry (see Figure S2). An unexpected observation was the presence of clearly defined iCAPs in the white matter, as FC is conventionally studied only for the gray matter. Despite the surprising character of these findings, there is compelling evidence that white matter has the vascular capacity to support hemodynamic changes and that the initial lack of interest in these signals was probably due to a limited sensitivity (lower field strength), rather than linked to a fundamental property that would impede their detection (Gawryluk et al., 2014; Gore et al., 2019). Indeed, recent studies reliably captured functionally relevant information in cerebral white matter (e.g., Ding et al., 2018; Huang et al., 2018; Peer et al., 2017; Wu et al., 2017). In the spinal cord, specifically, weaker BOLD signals in the white matter might be compensated by its large volume (i.e., more than three times the gray matter volume, see Figure S2). Coherent activity has previously been reported in

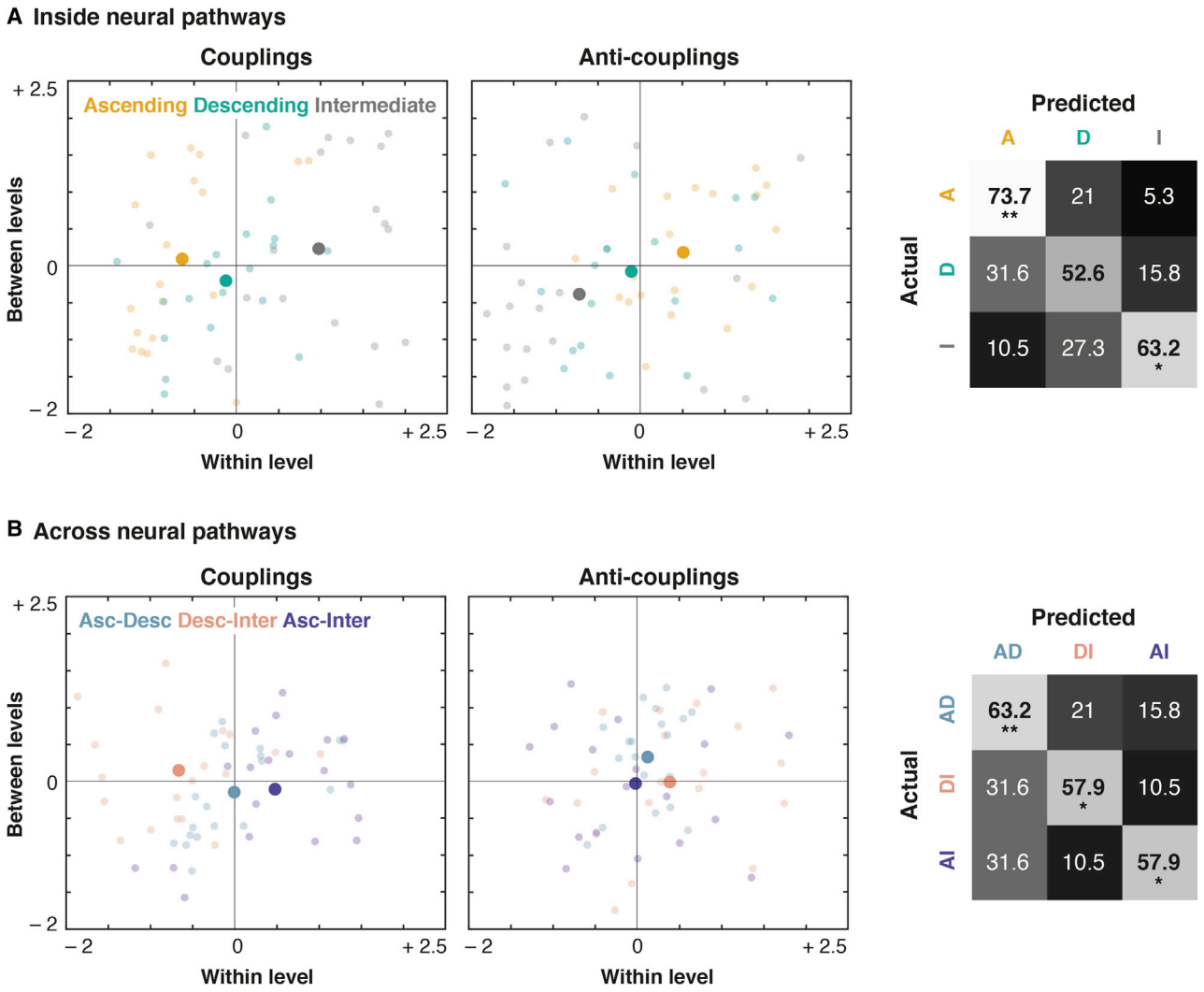

Figure 6. Interaction Signatures of Neural Pathways

To highlight whether couplings had a specific organization pertaining to neural pathways, we studied interactions inside (A) or across them (B). Patterns were highlighted based on four features: couplings and anti-couplings, both within level and between levels. Left: interactions in this feature space. Scatterplots show the relationship of within-level and between-level couplings and anti-couplings. Values are presented separately for the different interaction types, represented by distinct colors. The light dots correspond to the values of individual subjects, and the bold dots indicate the means over subjects. The distinct distributions of these values for each interaction type suggested that specific interaction signatures exist for the different neural pathways. To confirm these signatures, a quadratic discriminant analysis (QDA) classifier (leave-one-subject-out cross validation) was used to distinguish them. The average confusion matrices are displayed on the right. *$p < 0.05$, **$p < 0.01$ (non-parametric permutation testing, corrected for multiple comparisons). Asc/A, ascending; Desc/D, descending; Inter/I, intermediate.

spinal white matter at rest, as Barry et al. (2014) observed correlations between white matter regions using a seed-based analysis. Besides, the ICA components presented by Kong et al. (2014) did not allow an accurate delineation between gray and white matter and seemingly contained both structures. Altogether, our findings illustrate the potential of a dFC framework to resolve functional activity with high precision, down to the level of individual gray and white matter regions. Importantly, this framework may offer valuable insight into neurological conditions principally affecting the white matter, such as multiple sclerosis. To evaluate the reliability of our approach, we probed the intra-subject robustness of spinal iCAPs by extracting components on split-half datasets (Figure 4A). The low-granularity architecture was particularly stable, and high-granularity iCAPs of both sets coincided with atlas regions. The latter indicated that short acquisitions already allowed us to recover meaningful fine-grained components and could be foreseen in the context of clinical applications, where time is often a limiting factor. By evaluating inter-subject similarity (Figure 4B), we then showed that low- and high-granularity iCAPs were stable across subjects, hence supporting the idea that they represent consistent features of spinal cord functional organization. It is noteworthy that low-granularity iCAPs were more stable within than between subjects. This finding could pertain to individual differences

regarding the location of spinal levels, as anatomical variability was, indeed, previously acknowledged (Cadotte et al., 2015). In contrast, high-granularity iCAPs were more similar between than within subjects. We hypothesized that fine-grained maps, as they capture regions involved in specific functions (e.g., proprioception or muscle tone control), were more likely to vary over time depending on external variations (e.g., fatigue, stress or muscle relaxation). Spinal FC was previously reported to be state dependent, for instance following thermal stimulation (Weber et al., 2018). Further studies with physiology-based measures of cognitive states (e.g., electroencephalography, blood pressure, skin conductance, and pupillometry) (Lohani et al., 2019) could help validate this conjecture.

The "Restless" Spinal Cord Is Organized According to Neural Pathways

To date, the mechanisms at the core of spinal RS fluctuations are still speculative. Three main processes have been hypothesized (Eippert et al., 2017b; Eippert and Tracey, 2014; Kong et al., 2014): (1) RS signals could be driven by the continuous processing of inputs from the periphery (e.g., proprioception, touch, or vibration); (2) alternatively, they potentially stem from the ongoing communication between the brain and the spinal cord, through ascending (sensory) and descending (motor) signals; (3) finally, they could be generated locally from intrinsic features of spinal activity, for instance linked to coordinated movements (e.g., bilateral coordination [Jankowska, 2008; Soteropoulos et al., 2013], breathing [Sandhu et al., 2015], or central pattern generators [Guertin and Steuer, 2009]). To further shed light on these three hypotheses, we inspected the functional roles of the fine-grained iCAPs. First of all, we found that, similarly to the brain (Fox and Raichle, 2007; Smith et al., 2009), RS spinal components were distributed in networks corresponding to distinct neural pathways, which are usually active and modulated during task. This finding suggests that, at the level of the spinal cord, the same neural substrates likely support active and passive behaviors. Specifically, networks were mainly involved in descending and ascending processes associated with two spinal neural pathways: the CST and the DCML (Figure 3). By conveying and processing signals from (e.g., for motor control) and to (e.g., for proprioception) the brain, respectively, these pathways subserve distinct functions (Darby and Frysztak, 2013). The CST is the major pathway supporting voluntary motor function, and it connects motor cortical regions to the ventral horns of the spinal cord. Conversely, the DCML is related to proprioception, fine touch, and vibration sensation. Peripheral signals originating from receptors involved in tactile sensation and conscious proprioception travel through the dorsal column and the medial lemniscus, before reaching the primary somatosensory cortex. Although other spinal pathways exist, they were not detected here, possibly due to their secondary role at rest. One such example is the reticulospinal tract, which is mainly involved in postural control (Figure S2). The absence of these pathways could also pertain to their small size, as the spatial resolution (1 × 1 × 3 mm) could have hindered their identification. A few components were observed in the intermediate region of the spinal cord and can be engaged in different mechanisms, such as commissural interneuronal connections between contralateral horns, for instance to coordinate movement (Jankowska, 2008; Soteropoulos et al., 2013). At the interface between ascending and descending pathways, they may also support an interaction between sensory and motor components, notably for reflexes (Koch, 2019; Pierrot-Deseilligny and Burke, 2005). From these findings, we could infer that the aforementioned mechanisms likely coexist and generate restless spinal cord activity.

To help further clarify the organizational principles of this dynamic architecture, we then considered the temporal characteristics of spinal iCAPs, which displayed a significant overlap (Figure 5A). Although strong couplings occurred mostly within the same spinal level, in line with earlier studies (Barry et al., 2014; Eippert et al., 2017b; Kong et al., 2014; Liu et al., 2016; Weber et al., 2018), anti-couplings were weaker and identified between spinal levels (Figures 5B–5D). Weak negative correlations between spinal segments were previously reported by Kong et al. (2014) and may be reminiscent of mechanisms involved in intersegmental inhibition (Friesen and Cang, 2001; McBain et al., 2016). Patterns of interactions specific to each neural pathway also emerged from this analysis (Figure 6). Successful classification of these pathway-dependent signatures further confirmed their specificity, highlighting that distinct pathways might rely on different dynamic interactions to achieve their functional contributions. The strongest level of couplings was found for iCAPs located in the intermediate zone, not only among them but also with regions of the ascending pathway. This finding suggests that ongoing communication between hemicords may occur through interneuronal connections and point to a potential role of the intermediate pathway in bridging sensory networks. Conversely, ascending and descending pathways appeared to be more loosely connected, maybe due to the absence of active task. This initial disentanglement of spinal neural pathways *in vivo* could help us understand the impact of task-related modulations on their interactions, for instance during the complex integration of sensory feedback and motor commands involved in voluntary movements. In this context, collecting behavioral data will be pivotal for further assessing the relevance of these networks.

Clinical Potential

In addition to these findings, the versatility of our framework could enable researchers to explore the disruption of spinal functional architecture in impaired individuals. Studies assessing spinal functional integrity may be especially valuable when structural damages are minimal and do not allow full characterization of the patient's status. Multiple sclerosis could particularly benefit from this approach, as its pathological hallmark is the formation of demyelinating lesions in the brain and spinal cord (Filippi et al., 2018). Recent work from Conrad et al. (2018) has already initiated this effort, with promising results. Using a region of interest correlation analysis in a cohort of multiple sclerosis patients, they showed that the presence of lesions was concomitant to local alterations of FC. They speculated that different mechanisms could explain these changes, such as a compensatory effect of white matter damage or a disruption of inhibitory spinal interneurons. Our data-driven approach could help resaerchers distinguish between these hypotheses, by granting access to fine-grained features of spinal

cord FC in the white and gray matter. In addition, studying functional integrity could also bring valuable knowledge in the context of spinal cord injuries. To this end, RS scans are particularly attractive, as even severely affected patients can undergo such recordings (Krakauer, 2007). No such study has so far been performed in humans, but the clinical relevance of RS fluctuations was investigated in non-human primates at ultra-high field (Chen et al., 2015) by longitudinally monitoring the effect of a unilateral spinal cord injury. This investigation emphasized that disruptions in FC within and between spinal levels were related to the recovery process, thus underscoring the potential of intrinsic RSNs as imaging biomarkers of spinal cord functional integrity. The framework proposed in our study offers the prospect of identifying such functional biomarkers in the human spinal cord with a remarkable level of detail. This benefit can have major translational implications, as these biomarkers could potentially be used for diagnosis and prognosis to quantify disease progression or to investigate the effect of different interventions. Ultimately, a thorough understanding of spinal functional circuitry could help steer the development of innovative therapies, notably in the context of neurotechnological solutions that are able to deliver precise and knowledge-based treatment (Micera et al., 2020). For instance, electrical epidural stimulation has been used to restore locomotion following a spinal cord injury, with very promising results (Wagner et al., 2018). Patient-specific maps of spinal pathways could be used to fine-tune these protocols, so as to optimally engage the spared connections and networks to further improve a patient's clinical outcome.

Conclusions

So far, studies have inspected spinal RS fluctuations only by using static FC, showing that signals were organized into networks, but without demonstrating their physiological origin. Here, we deployed the SpiCiCAP framework to exploit the rich dynamic features of spontaneous spinal activity and recovered fine-grained components. Capitalizing on this unprecedented level of detail, we showed that these components were related to the underlying neuroanatomical organization and that they were functionally relevant. We provide a powerful tool to delineate stable spinal circuits *in vivo*, thus enabling access to the building blocks of spinal functional activity. This approach provides a foundation for future work to elucidate how spinal networks can be flexibly combined to support particular functions, both at rest or when specifically modulated by a task. We believe that the versatility of this methodological framework opens new avenues to tackle fundamental and clinical neuroscientific questions related to the function of the spinal cord.

STAR★METHODS

Detailed methods are provided in the online version of this paper and include the following:

- KEY RESOURCES TABLE
- RESOURCE AVAILABILITY
  - Lead Contact
  - Materials Availability
  - Data and Code Availability
- EXPERIMENTAL MODEL AND SUBJECT DETAILS
- METHOD DETAILS
  - Data acquisition
- QUANTIFICATION AND STATISTICAL ANALYSIS
  - Data processing
  - Data analysis

SUPPLEMENTAL INFORMATION

Supplemental Information can be found online at https://doi.org/10.1016/j.neuron.2020.07.024.

ACKNOWLEDGMENTS

We thank Loan Mattera and Roberto Martuzzi for their help with the acquisitions. This study was partly funded by the Wyss Center for Bio and Neuroengineering, the Swiss National Competence Center Research (NCCR) Robotics, the grant number 2017-205 of the Strategic Focal Area "Personalized Health and Related Technologies" of the ETH Domain, and the Bertarelli Foundation. This work was also supported by the Fondation Campus Biotech Geneva.

AUTHOR CONTRIBUTIONS

N.K., E.P., S.M., and D.V.d.V. initiated the study and wrote the paper. N.K. and E.P. designed the protocol and collected the data. N.K. processed and analyzed the data.

DECLARATION OF INTERESTS

The authors declare no competing interests.

Received: May 4, 2020
Revised: June 23, 2020
Accepted: July 18, 2020
Published: September 9, 2020

REFERENCES

Allali, G., Blumen, H.M., Devanne, H., Pirondini, E., Delval, A., and Van De Ville, D. (2018). Brain imaging of locomotion in neurological conditions. Neurophysiol. Clin. *48*, 337–359.

Barry, R.L., Smith, S.A., Dula, A.N., and Gore, J.C. (2014). Resting state functional connectivity in the human spinal cord. eLife *3*, e02812.

Barry, R.L., Rogers, B.P., Conrad, B.N., Smith, S.A., and Gore, J.C. (2016). Reproducibility of resting state spinal cord networks in healthy volunteers at 7 Tesla. Neuroimage *133*, 31–40.

Barry, R.L., Conrad, B.N., Smith, S.A., and Gore, J.C. (2018). A practical protocol for measurements of spinal cord functional connectivity. Sci. Rep. *8*, 16512.

Brooks, J.C.W., Beckmann, C.F., Miller, K.L., Wise, R.G., Porro, C.A., Tracey, I., and Jenkinson, M. (2008). Physiological noise modelling for spinal functional magnetic resonance imaging studies. Neuroimage *39*, 680–692.

Cadotte, D.W., Cadotte, A., Cohen-Adad, J., Fleet, D., Livne, M., Wilson, J.R., Mikulis, D., Nugaeva, N., and Fehlings, M.G. (2015). Characterizing the location of spinal and vertebral levels in the human cervical spinal cord. AJNR Am. J. Neuroradiol. *36*, 803–810.

Calhoun, V.D., Adali, T., Pearlson, G.D., and Pekar, J.J. (2001). A method for making group inferences from functional MRI data using independent component analysis. Hum. Brain Mapp. *14*, 140–151.

Castellanos, F.X., Di Martino, A., Craddock, R.C., Mehta, A.D., and Milham, M.P. (2013). Clinical applications of the functional connectome. Neuroimage *80*, 527–540.

Chen, L.M., Mishra, A., Yang, P.-F., Wang, F., and Gore, J.C. (2015). Injury alters intrinsic functional connectivity within the primate spinal cord. Proc. Natl. Acad. Sci. USA *112*, 5991–5996.

Conrad, B.N., Barry, R.L., Rogers, B.P., Maki, S., Mishra, A., Thukral, S., Sriram, S., Bhatia, A., Pawate, S., Gore, J.C., and Smith, S.A. (2018). Multiple sclerosis lesions affect intrinsic functional connectivity of the spinal cord. Brain *141*, 1650–1664.

Damoiseaux, J.S., Rombouts, S.A.R.B., Barkhof, F., Scheltens, P., Stam, C.J., Smith, S.M., and Beckmann, C.F. (2006). Consistent resting-state networks. Proc. Natl. Acad. Sci. USA *103*, 13848–13853.

Darby, S.A., and Frysztak, R.J. (2013). Neuroanatomy of the spinal cord. In Clinical Anatomy of the Spine, Spinal Cord, and ANS, Third Edit. (Elsevier Inc.).

De Leener, B., Lévy, S., Dupont, S.M., Fonov, V.S., Stikov, N., Louis Collins, D., Callot, V., and Cohen-Adad, J. (2017). SCT: Spinal Cord Toolbox, an open-source software for processing spinal cord MRI data. Neuroimage *145*, 24–43.

De Leener, B., Fonov, V.S., Collins, D.L., Callot, V., Stikov, N., and Cohen-Adad, J. (2018). PAM50: Unbiased multimodal template of the brainstem and spinal cord aligned with the ICBM152 space. Neuroimage *165*, 170–179.

Ding, Z., Huang, Y., Bailey, S.K., Gao, Y., Cutting, L.E., Rogers, B.P., Newton, A.T., and Gore, J.C. (2018). Detection of synchronous brain activity in white matter tracts at rest and under functional loading. Proc. Natl. Acad. Sci. USA *115*, 595–600.

Eippert, F., and Tracey, I. (2014). The spinal cord is never at rest. eLife *3*, e03811.

Eippert, F., Kong, Y., Jenkinson, M., Tracey, I., and Brooks, J.C.W. (2017a). Denoising spinal cord fMRI data: Approaches to acquisition and analysis. Neuroimage *154*, 255–266.

Eippert, F., Kong, Y., Winkler, A.M., Andersson, J.L., Finsterbusch, J., Büchel, C., Brooks, J.C.W., and Tracey, I. (2017b). Investigating resting-state functional connectivity in the cervical spinal cord at 3T. Neuroimage *147*, 589–601.

Filippi, M., Bar-Or, A., Piehl, F., Preziosa, P., Solari, A., Vukusic, S., and Rocca, M.A. (2018). Multiple sclerosis. Nat. Rev. Dis. Primers *4*, 43.

Finsterbusch, J. (2013). Functional neuroimaging of inner fields-of-view with 2D-selective RF excitations. Magn. Reson. Imaging *31*, 1228–1235.

Finsterbusch, J., Eippert, F., and Büchel, C. (2012). Single, slice-specific z-shim gradient pulses improve T2*-weighted imaging of the spinal cord. Neuroimage *59*, 2307–2315.

Fox, M.D., and Raichle, M.E. (2007). Spontaneous fluctuations in brain activity observed with functional magnetic resonance imaging. Nat. Rev. Neurosci. *8*, 700–711.

Friesen, W.O., and Cang, J. (2001). Sensory and central mechanisms control intersegmental coordination. Curr. Opin. Neurobiol. *11*, 678–683.

Gawryluk, J.R., Mazerolle, E.L., and D'Arcy, R.C.N. (2014). Does functional MRI detect activation in white matter? A review of emerging evidence, issues, and future directions. Front. Neurosci. *8*, 239.

Giove, F., Garreffa, G., Giulietti, G., Mangia, S., Colonnese, C., and Maraviglia, B. (2004). Issues about the fMRI of the human spinal cord. Magn. Reson. Imaging *22*, 1505–1516.

Giulietti, G., Giove, F., Garreffa, G., Colonnese, C., Mangia, S., and Maraviglia, B. (2008). Characterization of the functional response in the human spinal cord: Impulse-response function and linearity. Neuroimage *42*, 626–634.

Glover, G.H., Li, T.Q., and Ress, D. (2000). Image-based method for retrospective correction of physiological motion effects in fMRI: RETROICOR. Magn. Reson. Med. *44*, 162–167.

Gore, J.C., Li, M., Gao, Y., Wu, T.L., Schilling, K.G., Huang, Y., Mishra, A., Newton, A.T., Rogers, B.P., Chen, L.M., et al. (2019). Functional MRI and resting state connectivity in white matter—a mini-review. Magn. Reson. Imaging *63*, 1–11.

Greenberg, S.A. (2003). The history of dermatome mapping. Arch. Neurol. *60*, 126–131.

Greicius, M.D., Krasnow, B., Reiss, A.L., and Menon, V. (2003). Functional connectivity in the resting brain: a network analysis of the default mode hypothesis. Proc. Natl. Acad. Sci. USA *100*, 253–258.

Guertin, P.A., and Steuer, I. (2009). Key central pattern generators of the spinal cord. J. Neurosci. Res. *87*, 2399–2405.

Hanwerker, D.A., Ollinger, J.M., and D'Esposito, M. (2004). Variation of BOLD hemodynamic responses across subjects and brain regions and their effects on statistical analyses. Neuroimage *21*, 1639–1651.

Huang, Y., Bailey, S.K., Wang, P., Cutting, L.E., Gore, J.C., and Ding, Z. (2018). Voxel-wise detection of functional networks in white matter. Neuroimage *183*, 544–552.

Jankowska, E. (2008). Spinal interneuronal networks in the cat: elementary components. Brain Res. Brain Res. Rev. *57*, 46–55.

Jenkinson, M., Beckmann, C.F., Behrens, T.E.J., Woolrich, M.W., and Smith, S.M. (2012). FSL. Neuroimage *62*, 782–790.

Karahanoğlu, F.I., and Van De Ville, D. (2015). Transient brain activity disentangles fMRI resting-state dynamics in terms of spatially and temporally overlapping networks. Nat. Commun. *6*, 7751.

Karahanoğlu, F.I., Caballero-Gaudes, C., Lazeyras, F., and Van de Ville, D. (2013). Total activation: fMRI deconvolution through spatio-temporal regularization. Neuroimage *73*, 121–134.

Kinany, N., Pirondini, E., Martuzzi, R., Mattera, L., Micera, S., and Van de Ville, D. (2019). Functional imaging of rostrocaudal spinal activity during upper limb motor tasks. Neuroimage *200*, 590–600.

Knikou, M. (2008). The H-reflex as a probe: pathways and pitfalls. J. Neurosci. Methods *171*, 1–12.

Koch, S.C. (2019). Motor task-selective spinal sensorimotor interneurons in mammalian circuits. Curr. Opin. Physiol. *8*, 129–135.

Kong, Y., Jenkinson, M., Andersson, J., Tracey, I., and Brooks, J.C.W. (2012). Assessment of physiological noise modelling methods for functional imaging of the spinal cord. Neuroimage *60*, 1538–1549.

Kong, Y., Eippert, F., Beckmann, C.F., Andersson, J., Finsterbusch, J., Büchel, C., Tracey, I., and Brooks, J.C.W. (2014). Intrinsically organized resting state networks in the human spinal cord. Proc. Natl. Acad. Sci. USA *111*, 18067–18072.

Krakauer, J.W. (2007). Avoiding performance and task confounds: multimodal investigation of brain reorganization after stroke rehabilitation. Exp. Neurol. *204*, 491–495.

Lévy, S., Benhamou, M., Naaman, C., Rainville, P., Callot, V., and Cohen-Adad, J. (2015). White matter atlas of the human spinal cord with estimation of partial volume effect. Neuroimage *119*, 262–271.

Li, M., Newton, A.T., Anderson, A.W., Ding, Z., and Gore, J.C. (2019). Characterization of the hemodynamic response function in white matter tracts for event-related fMRI. Nature Communications *10*, 1–11.

Liégeois, R., Li, J., Kong, R., Orban, C., Van De Ville, D., Ge, T., Sabuncu, M.R., and Yeo, B.T.T. (2019). Resting brain dynamics at different timescales capture distinct aspects of human behavior. Nat. Commun. *10*, 2317.

Liu, X., Zhou, F., Li, X., Qian, W., Cui, J., Zhou, I.Y., Luk, K.D.K., Wu, E.X., and Hu, Y. (2016). Organization of the intrinsic functional network in the cervical spinal cord: A resting state functional MRI study. Neuroscience *336*, 30–38.

Logothetis, N.K., Pauls, J., Augath, M., Trinath, T., and Oeltermann, A. (2001). Neurophysiological investigation of the basis of the fMRI signal. Nature *412*, 150–157.

Lohani, M., Payne, B.R., and Strayer, D.L. (2019). A review of psychophysiological measures to assess cognitive states in real-world driving. Front. Hum. Neurosci. *13*, 57.

Marieb, E.N., and Hoehn, K.N. (2014). Human Anatomy & Physiology (Pearson).

McBain, R.A., Taylor, J.L., Gorman, R.B., Gandevia, S.C., and Butler, J.E. (2016). Human intersegmental reflexes from intercostal afferents to scalene muscles. Exp. Physiol. *101*, 1301–1308.

Micera, S., Caleo, M., Chisari, C., Hummel, F.C., and Pedrocchi, A. (2020). Advanced Neurotechnologies for the Restoration of Motor Function. Neuron *105*, 604–620.

Peer, M., Nitzan, M., Bick, A.S., Levin, N., and Arzy, S. (2017). Evidence for functional networks within the human brain's white matter. J. Neurosci. *37*, 6394–6407.

Piché, M., Cohen-Adad, J., Nejad, M.K., Perlbarg, V., Xie, G., Beaudoin, G., Benali, H., and Rainville, P. (2009). Characterization of cardiac-related noise in fMRI of the cervical spinal cord. Magn. Reson. Imaging *27*, 300–310.

Pierrot-Desseilligny, E., and Burke, D. (2005). The circuitry of the human spinal cord: its role in motor control and movement disorders (Cambridge University Press).

Power, J.D., Mitra, A., Laumann, T.O., Snyder, A.Z., Schlaggar, B.L., and Petersen, S.E. (2014). Methods to detect, characterize, and remove motion artifact in resting state fMRI. Neuroimage *84*, 320–341.

Powers, J.M., Ioachim, G., and Stroman, P.W. (2018). Ten key insights into the use of spinal cord fMRI. Brain Sci. *8*, 173.

Preti, M.G., Bolton, T.A., and Van De Ville, D. (2016). The dynamic functional connectome: State-of-the-art and perspectives. Neuroimage *160*, 41–54.

Sandhu, M.S., Baekey, D.M., Maling, N.G., Sanchez, J.C., Reier, P.J., and Fuller, D.D. (2015). Midcervical neuronal discharge patterns during and following hypoxia. J. Neurophysiol. *113*, 2091–2101.

Smith, S.M., Fox, P.T., Miller, K.L., Glahn, D.C., Fox, P.M., Mackay, C.E., Filippini, N., Watkins, K.E., Toro, R., Laird, A.R., and Beckmann, C.F. (2009). Correspondence of the brain's functional architecture during activation and rest. Proc. Natl. Acad. Sci. USA *106*, 13040–13045.

Soteropoulos, D.S., Edgley, S.A., and Baker, S.N. (2013). Spinal commissural connections to motoneurons controlling the primate hand and wrist. J. Neurosci. *33*, 9614–9625.

Stroman, P.W., Wheeler-Kingshott, C., Bacon, M., Schwab, J.M., Bosma, R., Brooks, J., Cadotte, D., Carlstedt, T., Ciccarelli, O., Cohen-Adad, J., et al. (2014). The current state-of-the-art of spinal cord imaging: methods. Neuroimage *84*, 1070–1081.

van den Heuvel, M.P., and Hulshoff Pol, H.E. (2010). Exploring the brain network: a review on resting-state fMRI functional connectivity. Eur. Neuropsychopharmacol. *20*, 519–534.

Vinh, N.X., Epps, J., and Bailey, J. (2010). Information theoretic measures for clusterings comparison: Variants, properties, normalization and correction for chance. J. Mach. Learn. Res. *11*, 2837–2854.

Wagner, F.B., Mignardot, J.-B., Le Goff-Mignardot, C.G., Demesmaeker, R., Komi, S., Capogrosso, M., Rowald, A., Seáñez, I., Caban, M., Pirondini, E., et al. (2018). Targeted neurotechnology restores walking in humans with spinal cord injury. Nature *563*, 65–71.

Weber, K.A., II, Sentis, A.I., Bernadel-Huey, O.N., Chen, Y., Wang, X., Parrish, T.B., and Mackey, S. (2018). Thermal Stimulation Alters Cervical Spinal Cord Functional Connectivity in Humans. Neuroscience *369*, 40–50.

Wheeler-Kingshott, C.A., Stroman, P.W., Schwab, J.M., Bacon, M., Bosma, R., Brooks, J., Cadotte, D.W., Carlstedt, T., Ciccarelli, O., Cohen-Adad, J., et al. (2014). The current state-of-the-art of spinal cord imaging: applications. Neuroimage *84*, 1082–1093.

Wu, X., Yang, Z., Bailey, S.K., Zhou, J., Cutting, L.E., Gore, J.C., and Ding, Z. (2017). Functional connectivity and activity of white matter in somatosensory pathways under tactile stimulations. Neuroimage *152*, 371–380.

Wu, T.L., Wang, F., Mishra, A., Wilson, G.H., 3rd, Byun, N., Chen, L.M., and Gore, J.C. (2018). Resting-state functional connectivity in the rat cervical spinal cord at 9.4 T. Magn. Reson. Med. *79*, 2773–2783.

Wu, T.L., Yang, P.F., Wang, F., Shi, Z., Mishra, A., Wu, R., Chen, L.M., and Gore, J.C. (2019). Intrinsic functional architecture of the non-human primate spinal cord derived from fMRI and electrophysiology. Nat. Commun. *10*, 1416.

Xu, R., and Wunsch, D., II. (2005). Survey of clustering algorithms. IEEE Trans. Neural Netw. *16*, 645–678.

Yakovenko, S., Mushahwar, V., VanderHorst, V., Holstege, G., and Prochazka, A. (2002). Spatiotemporal activation of lumbosacral motoneurons in the locomotor step cycle. J. Neurophysiol. *87*, 1542–1553.

STAR★METHODS

KEY RESOURCES TABLE

REAGENT or RESOURCE	SOURCE	IDENTIFIER
Deposited Data		
Raw and processed MRI data	This paper	https://doi.org/10.17632/n2k7zz2xyt.1
Software and Algorithms		
Processing & analysis pipeline (SpiCiCAP framework)	This paper	https://doi.org/10.17632/n2k7zz2xyt.1
MATLAB	Mathworks	RRID: SCR_001622 https://www.mathworks.com/
FSL	Jenkinson et al., 2012	RRID: SCR_002823 https://fsl.fmrib.ox.ac.uk/fsl/fslwiki
Spinal Cord Toolbox	De Leener et al., 2017	RRID:SCR_014170 https://github.com/neuropoly/spinalcordtoolbox
iCAP toolbox	Karahanoğlu and Van De Ville, 2015	https://c4science.ch/source/iCAPs/

RESOURCE AVAILABILITY

Lead Contact

Further information and requests for resources should be directed to and will be fulfilled by the Lead Contact, Prof. Dimitri Van De Ville (dimitri.vandeville@epfl.ch).

Materials Availability

This study did not generate new unique reagents.

Data and Code Availability

Original data have been deposited to Mendeley Data: https://doi.org/10.17632/n2k7zz2xyt.1, along with codes generated in this study https://doi.org/10.17632/n2k7zz2xyt.1.

EXPERIMENTAL MODEL AND SUBJECT DETAILS

Twenty-two right-handed healthy subjects (11 females, 28.5 ± 3.5 years old) were enrolled in the study. All participants gave their written informed consent to participate, and the study had been approved by the Commission Cantonale d'Éthique de la Recherche Genève (CCER, study 2019-00203). All volunteers had normal or corrected-to-normal vision and no history of neurological disorders

METHOD DETAILS

Data acquisition

The imaging protocol was the same as the one used in our previous study in which we imaged the rostrocaudal patterns of activity elicited by upper limb movements (Kinany et al., 2019). Imaging data were acquired with a 3.0 Tesla Siemens Prisma scanner (Erlangen, Germany), equipped with a 64-channel head (only inferior element, HC7, was used) and neck coil (both anterior and posterior elements, NC1 and NC2, were used – i.e., 24 channels). For 14 subjects, the upper element of the spine coil (SP1) was also used (optimal coil combination defined by the scanner). All functional acquisitions were performed with a gradient-echo echo-planar sequence, with ZOOMit selective field-of-view imaging (Repetition Time (TR) = 2.5 s, Echo Time (TE) = 34 ms, FOV = 48 × 144 mm, flip angle = 80°, in-plane resolution = 1 × 1 mm, slice thickness = 3 mm). The cervical enlargement was covered using 32 axial slices. Particular care was taken in placing slices perpendicularly to the spinal cord, in order to maximize the alignment with the intervertebral discs and limit signal dropouts due to field inhomogeneities (Finsterbusch et al., 2012). Before acquisition, the magnetic field homogeneity was optimized using shimming adjustments focused on the spinal cord. For each participant, 360 volumes (i.e., 15 minutes) were acquired, during rest (i.e., no explicit task), with eyes open (an empty screen was shown). A high-resolution T2-weighted anatomical image, covering a region from C1 to the upper part of the thoracic spine, was also acquired with a SPACE sequence (single slab 3D turbo spin echo sequence with a slab selective, variable excitation pulse, TR = 1500 ms, TE = 135 ms, echo train length = 74, flip angle = 140°, resolution = 0.4 × 0.4 × 0.8 mm, sagittal orientation). Throughout the recordings, subjects were instructed to relax, breathe normally and minimize motion. A soft cervical collar was used in order to stabilize the neck.

QUANTIFICATION AND STATISTICAL ANALYSIS

Data processing

All preprocessing steps were performed using the Oxford Center for fMRI of the Brain's (FMRIB) Software Library (FSL, version 5.0) (Jenkinson et al., 2012) and the Spinal Cord Toolbox (SCT, version 3.2.7) (De Leener et al., 2017). The pipeline is based on the one used in our previous study (Kinany et al., 2019).

1) Motion correction

All functional and anatomical images were inspected for potential artifacts. For each participant, the bottom slices whose signal was insufficient to accurately detect the spinal cord were removed. The mean functional image was then used to automatically detect the centerline of the spinal cord. A cylindrical mask (diameter of 30 mm) along the centerline was generated to prevent the inclusion of regions moving independently from the spinal cord and slice-wise realignment was performed with the mean functional image as reference. This procedure allows to account for the articulated structure of the spinal cord (De Leener et al., 2017). Motion parameters were extracted and used to compute the mean (i.e., average over slices and volumes) framewise displacement along the *x* and *y* directions (FD_x and FD_y). A stringent threshold on the framewise displacement (i.e., mean FD_x or $FD_y > 0.2$ mm) was applied to detect subjects with excessive motion. This led to the exclusion of three subjects. All the other subjects (n = 19) were included in further analyses. The overall level of motion of these remaining subjects was minimal (mean ± SE along *x* and *y*: $FD_x = 0.10 \pm 0.04$ mm, and $FD_y = 0.10 \pm 0.03$ mm).

Following slice-wise realignment, outliers volumes were detected for motion scrubbing (i.e., to be included as noise regressors during the time courses denoising, see *2) Denoising time courses*). Variations in image intensity were assessed to identify potential outliers with FSL, using DVARS (i.e., the root mean square intensity difference of volume N to volume N+1) within the spinal cord, and a box-plot cutoff (75th percentile + 1.5 x the interquartile range) (Power et al., 2014). On average, five volumes per run were considered as outliers.

2) Denoising time courses

Due to the proximity of respiratory tracts and visceral organs, the spinal cord is particularly prone to physiological motion (Brooks et al., 2008; Eippert et al., 2017a; Piché et al., 2009). It is, therefore, essential to limit the detrimental impact of those fluctuations on BOLD time courses. For this purpose, physiological signals (i.e., heart rate and respiration) and scanner triggers were acquired throughout the functional scans, using a photoplethysmograph and a respiratory belt (Biopac MP150 system, California, USA). These recordings were used to generate noise regressors, with a procedure based on RETROspective Image CORrection (RETROICOR) (Glover et al., 2000). Briefly, this approach assigns cardiac and respiratory phases to each functional volume, considering their acquisition timings with respect to the physiological traces. Then, a low-order Fourier expansion is typically used to model physiological noise. In the spinal cord, however, recommendations suggest to include higher order Fourier terms as well as the noise related to the cerebrospinal fluid (CSF) (Brooks et al., 2008; Kong et al., 2012). Accordingly, we generated 32 voxelwise noise regressors using the physiological noise modeling (PNM) tool from FSL, along with an additional regressor corresponding to the CSF signal (mean signal in the 10% of CSF voxels whose signal varies the most).

These 33 physiological noise regressors (PNM and CSF) were combined with motion correction parameters (i.e., two slice-wise regressors, for the motion in *x* and *y*) and motion outliers (see 1) Motion correction), and regressed from the fMRI time-series using FSL's fMRI Expert Analysis Tool (FEAT). The resulting residuals were then spatially smoothed using a 3D Gaussian kernel with a full width half maximum (FWHM) of 2 × 2 x 6 mm^3. Smoothing was performed along the centerline of the spinal cord, so as to preserve anatomical consistency.

3) Estimating warping fields for normalization

The PAM50 template (spatial resolution of 0.5 × 0.5 × 0.5mm^3) was employed as a common space (De Leener et al., 2018). Using the Spinal Cord Toolbox (De Leener et al., 2017), a two-step registration procedure was performed for each subject: i) *Anatomical-to-template*: automatic spinal cord segmentation and vertebrae labeling was performed, based on the T2-weighted image. The spinal cord was then straightened along its centerline and registered to the PAM50 template, using the labels (specifically for the vertebral bodies C4 and C7) and non-rigid transformations; ii) *Functional-to-anatomical:* functional images were registered to the T2-weighted image, using non-rigid transformations. The warping fields from steps i) and ii) were finally concatenated to obtain the *functional-to-template* transformation. Accurate spatial registration to a common space is a crucial step to allow meaningful inter-subject comparison. Nevertheless, the normalization procedure in the spinal cord is notoriously challenging, partly because of its small size, combined with non-uniform signal quality (Giove et al., 2004). To validate the precision of our registration to the PAM50 template, we show the results of this procedure in Figure S1, which illustrates the accurate correspondence between the normalized anatomical and functional images and the template. Importantly, the delineation between gray and white matter can be clearly observed in the normalized fMRI runs.

Data analysis

1) Extracting innovation-driven coactivation patterns (iCAPs)

The innovation-driven co-activation patterns (iCAPs) pipeline was performed using the iCAP toolbox (MATLAB code openly available on https://c4science.ch/source/iCAPs/; Karahanoğlu and Van De Ville, 2015). The different steps of the pipeline are illustrated in Figure 1. In detail, the measured fMRI time course is assumed to reflect the underlying activity-inducing signal, temporally smoothed by

the effect of the hemodynamic response function (HRF). As a result, we first used the denoised images (native space) and deployed a regularized deconvolution, using the Total Activation framework (TA; Karahanoğlu et al., 2013), to reliably retrieve these activity-inducing signals. Transients (i.e., the so-called innovation signals) were computed as the temporal derivative of these activity-inducing time courses. It is worth highlighting that innovation frames present spatial patterns that are much cleaner than the related fMRI frames because they have been undone from hemodynamic blur, but also noise that is not compatible with the hemodynamic properties. In order to select significant innovations (i.e., frames with significant transitioning activities), a two-step thresholding procedure was used: i) temporal thresholding: for each voxel, a surrogate distribution was obtained by applying TA on phase randomized data and a 5% confidence interval was used to select significant voxels, ii) spatial thresholding: only the innovation frames with at least 5% of active voxels were considered to be significant. Significant innovation frames were normalized to the PAM50 and used to identify resting-state components, the iCAPs, using temporal K-means clustering. Two levels of granularity were chosen: i) K = 4 (low granularity) and ii) K = 40 (high granularity). The iCAPs spatial maps were then thresholded ($Z > 1.6$ for K = 4 and $Z > 5$ for K = 40) and binarized, and their spatial similarity evaluated by means of Dice coefficients (i.e., twice the overlapping area, divided by the total number of voxels in both maps).

It should be pointed out that *a priori* estimating data dimensionality is a long standing issue in network analyses (Xu and Wunsch, 2005). In order to ensure that selecting 4 low-granularity and 40 high-granularity components provided reliable partitions of the data, we systematically evaluated the reproducibility of the clustering for different values of K (see Figure S3). Specifically, we used a subsampling scheme where clustering was repeated using random subsets of the data (100 subsets of 10 subjects). For each repetition, K-means clustering was performed using different values of K and each clustering solution was compared to the global clustering obtained with the 19 subjects, using the adjusted mutual information (AMI) (Vinh et al., 2010) which estimates the similarity of two discrete assignments (i.e., by comparing the assignments of the significant innovation frames to the different clusters). Of note, this metric is corrected for the effect of chance in order to avoid biasing results in favor of a large number of clusters. Values range from 0 (chance level) to 1 (equal partitions). In order to explore low-granularity values, K values corresponding to multiples of four (i.e., number of spinal levels in the imaged regions) were probed. Moreover, we investigated higher values of K, ranging from 20 to 90 in steps of 10, hence covering a wide range of potential fine-grained subdivisions. Details of this analysis are presented in Figure S3.

2) Linking iCAPs with spinal levels and atlas regions

To validate the relevance of the iCAP spatial patterns, we assessed whether they were related to the underlying neuroanatomy of the spinal cord. In order to do so, we relied on probabilistic atlas maps provided by the Spinal Cord Toolbox (De Leener et al., 2017), including both spinal levels (Cadotte et al., 2015) and atlas regions (Lévy et al., 2015) (see Figure S2). To investigate the spatial distribution of the low- and high-granularity iCAPs, we used binarized versions of the probabilistic atlas maps and computed, for each iCAP, the proportion of voxels found in the different levels and regions. As the aim was to precisely localize spatial maps with respect to the atlas regions, atlas maps were thresholded at a probability of 0.5 before binarization, to ensure that only the highest probabilities were taken into account for the assignment. Based on these distributions, low- and high-granularity iCAPs were then uniquely matched to individual spinal levels or atlas regions, respectively, using a hard assignment based on the maximum number of voxels. Dice coefficients were used to confirm the accuracy of the matching. To this end, the full extent of the corresponding atlas maps was considered (i.e., non-zero probability), so as to assess the correspondence between borders. Finally, fine-grained iCAPs were grouped based on their neuroanatomical identity. For presentation purposes, iCAPs were ordered rostro-caudally based on the location of their center-of-gravity, unless indicated otherwise.

3) Assessing iCAP stability

We assessed iCAPs stability within and between subjects. In order to investigate the temporal stability over all subjects (i.e., stability within subjects), we assessed the *intra-subject* similarity. For each subject, the functional run was split into two equal parts of 7.5 minutes (i.e., 180 volumes). The procedure to obtain iCAP maps was performed independently for these two parts and using both levels of granularity (K = 4 or 40). Dice coefficients were computed to assess the similarity between the spatial maps of the two parts. To ensure that the spatial organization of iCAPs was stable across subjects on the entire dataset (i.e., stability between subjects), we computed the *inter-subject* similarity, as the mean Dice coefficients over each pair of subjects, for a particular iCAP pair. For each subject, subject-wise iCAP maps were computed as the mean over the frames of this subject assigned to each iCAP and binarized ($Z > 3$).

4) Extracting temporal dynamics

Finally, subject-specific time courses were obtained by regional averaging of the activity-inducing signals within the binarized iCAP maps. In order to extract their temporal properties, the subject-level iCAPs time courses were Z-scored and thresholded ($|Z| > 1$) to highlight active and de-active time points. The total and average durations of each iCAP were computed, as well as couplings and anti-couplings between pairs of iCAPs, based on the number of time points with same signs or different signs simultaneous coactivations, expressed as Jaccard indices (i.e., percent joint activation time). To evaluate the statistical significance of these (anti-)couplings, we performed non-parametric permutation tests. At each permutation (n = 5000), we randomly assigned iCAP labels, for each subject and computed (anti)-couplings using Jaccard indices. The mean overall couplings (or anti-couplings) matrix over subjects was then calculated. The upper triangular matrices resulting from each permutation were finally used to build a null distribution on which thresholds for significance were obtained. Bonferroni correction (n = 2) was applied to account for the presence of both couplings and anti-couplings. Mean durations and couplings were compared using paired t tests (Bonferroni corrected).

5) Investigating neural interplays

In order to investigate whether interplays were functionally relevant, we studied interactions inside (between iCAPs of one pathway) and across (between iCAPs of different pathways) neural pathways (as defined based on the neuroanatomical identity of iCAPs, see *2) Linking iCAPs with spinal levels and atlas regions*). Interactions were described using four features (couplings and anti-couplings, both within and between levels). Values were Z-scored for each subject and feature and scatterplots were used to capture potential interaction signatures. To further assess whether these signatures were pathway-specific, three-class quadratic discriminant analysis (QDA) classifiers were employed, with leave-one-subject-out cross validation. Confusion matrices were computed considering all cross validation folds to summarize the accuracy of the classification. Statistical significance of accuracy was verified by performing non-parametric permutation testing. Specifically, classification was performed using the same procedure, but with randomly assigned labels. For each permutation (n = 5000), the three diagonal elements of the resulting confusion matrix were retrieved and used to build a null distribution on which thresholds for significance were obtained. As both interactions inside and across pathways were considered, Bonferroni correction was applied to account for the two comparisons.